Journal of Clinical & Experimental Cardiology

Thomas-Seale et al., J Clin Exp Cardiolog 2016, 7:12
DOI: 10.4172/2155-9880.1000481

Research Article Open Access

# Magnetic Resonance Elastography through Atherosclerosis: A Feasibility Study

**Thomas-Seale LEJ[1]*, Kennedy P[2], Hollis L[1], Hammer S[3], Anderson T[1], Mirsadraee S[2], Klatt D[4], Sack I[4], Pankaj P[5], Roberts N[2] and Hoskins PR[1]**

[1]*Centre for Cardiovascular Science, University of Edinburgh, Queen's Medical Research Institute, 47 Little France, Crescent, Edinburgh, EH16 4TJ, UK*
[2]*Clinical Research Imaging Centre, University of Edinburgh, 47 Little France Crescent, Edinburgh, EH16 4TJ, UK*
[3]*School of Engineering and Physical Sciences, Heriot-Watt University, Edinburgh, EH14 4AS, UK*
[4]*Department of Radiology, Charité - Universitätsmedizin Berlin, Berlin, Germany*
[5]*School of Engineering, University of Edinburgh, Alexander Graham Bell Building, The King's Buildings, Edinburgh, EH9 3JU, UK*

## Abstract

It is widely acknowledged that assessing the rupture risk of atherosclerotic plaques, via lumen reduction, is an imperfect criterion and that other properties such as those related to biomechanics may be more relevant. This study investigated the hypothesis that magnetic resonance elastography (MRE) can be used to image the elasticity of atherosclerotic plaques with the aim to give a better indication of rupture risk.

Atherosclerotic plaques were imaged through a small feasibility data set including stenosed arterial phantoms, healthy volunteers and peripheral artery disease (PAD) patients. Comparison of the healthy volunteer and PAD patient wave displacement images showed differences in noise levels, wave amplitudes and wave propagation through the lumen. However, the change in shear moduli through healthy and diseased areas of the phantoms and *in vivo* subjects could not be detected. Synthetic modelling of the arterial phantoms, under replicated imaging conditions, suggested that there is scope to improve the results through increased control of the phantom and the inclusion of more realistic blood mimic.

The MRE wave displacement appeared highly damped through the lumen of the atherosclerotic PAD data sets when compared to the healthy volunteers. This interesting result indicates that the presences of disease, likely to be calcified plaques, are causing changes in the wave propagation that may be captured using MRE. There is scope to clarify the conclusions in this study by developing the technique, particularly the imaging acquisition parameters and inversion algorithm.

**Keywords:** Arterial elastography; Atherosclerosis; Cardiovascular disease; FEA; MRI; MRE; Peripheral artery disease; Shear wave imaging

## Introduction

Atherosclerosis is the root cause of the majority of cardiovascular diseases (CVD) [1]. Although the pathogenesis of the disease is extremely complex [2,3], atherosclerosis is characterized by an accumulation of low density lipoproteins in the vascular wall. The development of the disease can lead to a narrowing of the lumen, known as a stenosis. Histologically, the American Heart Association classifies the advancement of a plaque by its composition [4,5]. Type VI lesions include those where thrombosis has been generated by exposure of the plaque core [5]. This clinical event is known as atherosclerotic plaque rupture and can lead to ischemia. The symptoms and severity of this depend on the location of the disease. The more severe consequences of atherosclerosis are heart attack and stroke, caused by ischemia in the coronary and carotid arteries respectively.

Clinical diagnosis, and the decision to surgically intervene, is made from a measurement of the stenosis and symptoms of ischemia [6]. Stenosis size is widely acknowledged as an imperfect surgical criterion. Rothwell et al. [7] pooled data from the North American Symptomatic Carotid Endarterectomy (NASCET) and European Carotid Surgery Trials (ECST) and found that 5 years post-surgery, the absolute risk reduction for 70-99% stenosis was only 18.7%. The vulnerability of a plaque to rupture is far more complex; involving size and composition of the lipid pool, and the thickness, mechanical properties, fatigue and inflammation of the fibrous cap [8].

The economic impact of CVD is huge. The annual direct and indirect costs are estimated to be $315 billion in the US [1] and £15 billion in the UK [9]. Improving the accuracy of atherosclerosis diagnosis is the focus of many avenues of research. Development of diagnostic techniques involves enhanced imaging of the plaque structure and mechanical properties [10-12]. More closely satisfying the clinical aim by identifying the vulnerability of an atherosclerotic plaque to rupture, offers the potential to reduce the global economic burden of CVD.

Magnetic resonance elastography (MRE) is a non-invasive elasticity imaging technique, which has the potential to differentiate between the mechanical properties of tissues. Phase-contrast magnetic resonance imaging (MRI) is used to capture the temporal and spatial propagation of low frequency, externally excited, harmonic waves through the tissue [13,14]. The mechanical properties are extracted from the displacement wave images using an inversion algorithm [14]. Experimentally, MRE has measured arterial wall stiffness using various inversion algorithms; the Moens-Korteweg [15-18] phase gradient [19] and local frequency estimation [20,21]. To date, the only application of

***Corresponding author:** Thomas-Seale LEJ, Department of Mechanical Engineering, School of Engineering, University of Birmingham, Edgbaston, Birmingham, B15 2TT, UK, Tel: (+44) 0121 4143622; E-mail: l.e.j.thomas-seale@bham.ac.uk / lauren.ej.thomas.seale@gmail.com

**Received** October 31, 2016; **Accepted** November 30, 2016; **Published** December 10, 2016

**Citation:** Thomas-Seale LEJ, Kennedy P, Hollis L, Hammer S, Anderson T, et al. (2016) Magnetic Resonance Elastography through Atherosclerosis: A Feasibility Study. J Clin Exp Cardiolog 7: 481. doi:10.4172/2155-9880.1000481

MRE to atherosclerosis has assessed stenosis size [15]. Recent advances in the technique have identified regional changes in the vascular wall, through phantoms and *ex vivo* [22]. Computational research, through synthetic data sets, has demonstrated that MRE has the potential to identify a contrast between the wave images [23] and shear moduli [24] of atherosclerotic plaque compositions.

Arterial phantoms are used extensively to test and validate imaging methods. In this study, experimental phantoms were developed using polyvinyl alcohol cryogel (PVA-c). This vessel mimicking material (VMM) is applicable to modelling atherosclerosis for the purpose of MRE imaging: it demonstrates elastic properties comparable with arterial tissue [25], a variable Young's modulus [26] and signal intensity and relaxation times well-suited to MRI [27]. PVA, in the form of a gel, transforms into a cryogel upon freezing and thawing, during which crystals grow and act as cross-linking sites [27]. PVA also demonstrates the ability to bond well with pre-manufactured PVA-c, making the design of heterogeneous vessel geometry possible. In previous studies, PVA-c has been used to create two dimensional changes in arterial wall stiffness [28] and three dimensional fibrous and lipid plaques [29,30].

The aim of this study is to assess the feasibility of applying MRE to atherosclerosis experimentally. This research will be the first application of MRE to atherosclerosis through arterial phantoms and peripheral artery disease (PAD) patients.

## Materials and Methods

### Arterial phantom design

Atherosclerotic plaques contain 2 main constituents; fibrous tissue and a lipid pool. Overlaying these is a fibrous cap which interfaces with the flowing blood. Stable plaques are mainly fibrous and unstable plaques have large lipid pool and/or thin cap. The experimental plaques in this study modelled the variation of mechanical properties with composition using 3 configurations; lipid, homogeneous and fibrous. The stenoses were modelled as 70% and eccentric. The vessels were embedded in a block of tissue mimicking material (TMM) to mimic the propagation of waves passing through tissue to the artery *in vivo*, Figure 1. Motion due to the cardiac cycle was neglected; the lumen was filled with water and assumed to remain static, beyond any interaction with the excitation wave.

**Vessel mimic manufacture:** The following methodology was applicable to the manufacture of the vessel walls and all three plaque types. 10% wt. PVA (PVAGELS, Kingston, NY, USA) was heated for 60 minutes in a water bath at 100 ± 1°C. The moulds were lubricated with silicon grease. PVA was injected into the moulds and left to stand for 24 h at room temperature. The freeze-thaw cycle involved a freezing stage at -20 ± 0.5°C for 14 h, followed by a thawing period at 22 ± 0.5°C, for 10 h [26]. The Young's modulus of PVA-c increases with the number of freeze-thaw cycles [26].

The shear modulus [26,31] and the geometric properties of the TMM and VMM are defined in Table 1. The healthy vessel wall and homogeneous atherosclerotic plaques were subjected to 3 freeze-thaw cycles [26]. To construct the homogeneous vessel a stenosis mould (Figure 1a) was held concentrically inside polyvinyl chloride tubing reinforced by an acrylic tube.

Fibrous plaques, relatively stiffer than the vessel wall, were manufactured prior to the vessel wall, using a plaque mould compatible with the stenosis moulds (Figure 1a). The fibrous plaque then underwent 2 freeze-thaw cycles. The stenosed rod, containing the plaque, was

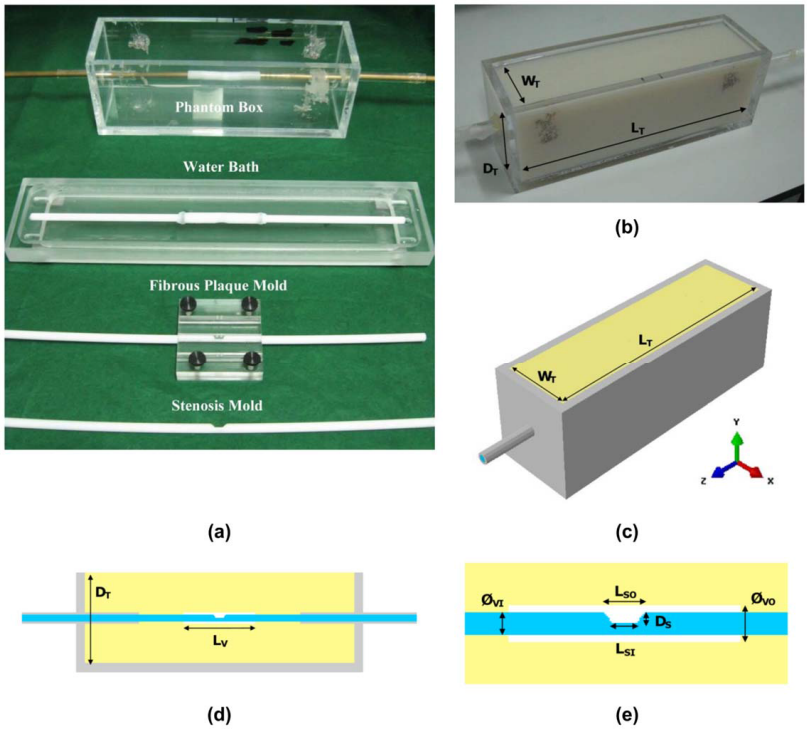


**Figure 1:** (a) Arterial phantom moulds and (b) completed arterial phantom. (c) Isometric view and (d) sectional view of phantom FEM. (d) Sectional view of the vessel geometry.

| Component of Phantom | | Material | | Geometry | | | | | |
|---|---|---|---|---|---|---|---|---|---|
| | | Type | Shear Modulus (kPa) | Length, L (mm) | | Width, W (mm) | Depth, D (mm) | Diameters, ø (mm) | |
| | | | | Inner, I | Outer, O | | | Inner, I | Outer, O |
| Surrounding Tissue, T | | Tissue Mimic | 16.8 [31] | N/A | 300 | 80 | 100 | N/A | N/A |
| Wall, V | | Vessel Mimic | 34.3 [26] | N/A | 80.0 | N/A | N/A | 8.0 | 13.0 |
| Stenosis, S | Fibrous | | 53.3 [26] | 8.0 | 13.0 | N/A | 5.6 | N/A | N/A |
| | Homogeneous | | 34.3 [26] | 8.0 | 13.0 | N/A | 5.6 | N/A | N/A |
| | Lipid | | 6.3 [26] | 8.0 | 13.0 | N/A | 5.6 | N/A | N/A |

**Table 1:** Geometric and Material Properties. (Nomenclature is referenced with respect to Figure 1).

aligned inside the vessel wall mould, as previously discussed, and surrounded by PVA. Three further freeze-thaw cycles were applied to this mould.

Lipid plaques were created with a stenosis less stiff than the wall. A healthy vessel wall was created using the previously described methodology and subjected to two freeze-thaw cycles. The PVA-c vessel was positioned around a stenosis mould and suspended in a water bath (Figure 1a). PVA gel was injected through the PVA-c wall into the stenosis hollow. The PVA-c was covered in water to prevent dehydration and subjected to one freeze-thaw cycle.

**Tissue mimic manufacture:** Each vessel was embedded in an agar based TMM, consisting of 1% wt. agar, 0.3% wt. preservative and water. The TMM ingredients were mixed and heated for one hour in a water bath at 96.9 ± 1°C and then allowed to cool to approximately 42°C. The PVA-c vessels were aligned with the lumen hollows and suspended in the phantom box using cylindrical rods (Figure 1a). The phantom was then filled with TMM, which upon cooling at room temperature for 12 h, changed from a liquid to a solid state. The rods supporting the PVA vessel were removed from the phantom and the lumen hollow was filled with water.

## Magnetic resonance imaging

Magnetic resonance imaging data was acquired using a 3T Verio imaging system (Siemens, Healthcare Gmbh, Erlangen, Germany). Elastography was conducted on 4 arterial phantoms, 2 healthy volunteers (HV1, HV2) and 3 PAD patients (P1, P2, P3).

**Angiography:** Magnetic resonance angiography (MRA) was required to identify the location of the region of interest (ROI). A Siemens 3D Native Space, echocardiogram triggered, non-contrast enhanced MRA acquisition was employed (Table 2). In the healthy volunteers, the ROI was defined as a clearly visible section of the femoral artery, isolated in the left leg. In the PAD patients the ROI was defined as the diseased section of artery.

**Elastography:** An actuator was used to transmit harmonic, sinusoidal waves to the ROI. A subwoofer loudspeaker (Carpower Raptor Mk-12, Monacor, Germany,) was used to generate the vibrations, which were transferred to the actuator by a carbon-fibre piston. The MRE equipment is shown in Figure 2. The smooth consistency and high water content of the agar based TMM made shear excitation of the phantoms impossible without causing significant damage to the phantom. Compressional excitation (parallel to the Y axis; Figure 1c) was employed and excessive vibration of the actuator was controlled by lightly constraining the piston. A finite, harmonic source exciting in the longitudinal direction intrinsically excites secondary waves in the other directions [32]. Compressional excitation has been shown to effectively excite mechanical waves that are compatible with MRE imaging and inversion [33]. The arterial phantoms were orientated with their long axes parallel to the bore of the scanner (Z direction; Figure 1c) and were imaged through the sagittal slice direction.

| | |
|---|---|
| **TR** | 930 ms |
| **TE** | 81 ms |
| **FoV** | 440 mm × 440 mm |
| **Matrix Size** | 384 × 384 |
| **Slice Thickness** | 1.3 mm |

**Table 2:** MRA Acquisition Parameters.

| | | |
|---|---|---|
| **Repetition Time** | | 1600 ms |
| **Echo Time** | | 56 ms |
| **Motion Encoding Gradient** | **Frequency** | 1 Hz |
| | **Amplitude** | 35 mT/m |
| **Peak to Peak Voltage** | | 4 V |
| **Field of View** | | 235 mm × 235 mm |
| **Matrix Size** | | 128 × 128 |
| **Slice Thickness** | | 10 mm |

**Table 3:** MRE Acquisition Parameters.

The excitation wave was transmitted to the arteries of the healthy volunteers and patients using the actuator shown in Figure 2c. The actuator was placed around the mid-upper thigh. With respect to patient comfort, the location of the actuator was matched as closely to the ROI as possible. Shear waves were generated parallel to the bore of the scanner (Z direction; Figure 1c). The subjects were imaged through the sagittal plane, rotated obliquely with respect to the transverse and coronal direction, to lie parallel to the vessel and through the ROI.

The MRE protocol utilised an echo planar imaging sequence with a motion encoding gradient, the protocol is outlined in Table 3. The excitation frequency was set at 100 Hz based on the successful results obtained Thomas-Seale et al. [24]. With reference to Figure 1c, the motion encoding directions are defined as follows; read out (RO) along the Y axis parallel to the compression wave, phase encoding (PE) along the Z axis parallel to the shear wave and slice select (SS) along the X axis. The acquisition yielded a series of magnitude and phase images, corresponding to images taken at time offsets through the steady state wave cycle: 40 for the arterial phantoms and 8 for the human subjects. The magnitude images were used to identify and isolate the ROI. The phase images were unwrapped, removing discontinuities generated when the phase falls outside of the $[-\pi, \pi)$ range [34], using Flynn's 2D minimum discontinuity algorithm [35]. The complex wave image, was extracted from the first harmonic of the temporally Fourier transformed phase images. These images served as the input to the inversion algorithm.

## Simulated arterial phantom

A synthetic data set was created using the methodology outlined in Thomas-Seale et al. [24]. This technique utilises a direct solution, steady state finite element (FE) analysis (Abaqus/CAE, Dassault Systèmes Simulia Corp., Providence, Rhode Island, USA) which allows the extraction of a complex wave image, analogous to the first harmonic

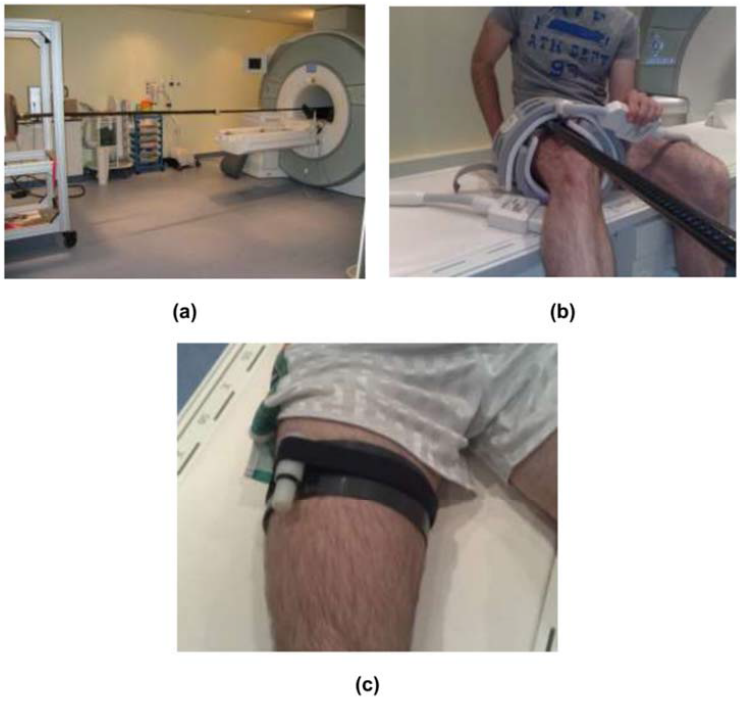


**Figure 2:** MRE equipment (a) subwoofer, piston and MRI scanner, (b) thigh actuator, piston and flex coil, (c) thigh actuator and piston attachment.

of the Fourier transformed phase images. The VMM and TMM were assumed incompressible and viscoelastic, represented by the Voigt model. The geometry (Rhinoceros version 3.0, McNeel, Seattle, Washington, USA) and material properties of the vessel and tissue mimic were replicated from those outlined in Table 1. Shear viscosity [36] and density [37] were given values of 3Pas and 1047 $kgm^{-3}$, respectively. The lumen was given the density and bulk modulus of water [38]; 1000 $kgm^{-3}$ and $2.2 \times 10^6$ kPa. The phantom container was modelled with a density and Young's Modulus of acrylic; 1180 $kgm^{-3}$ and $3.2 \times 10^6$ kPa. The resulting FE model is described in Figure 1.

The excitation nodes represented the contact area and location of the actuator on the arterial phantom. A load of 10N was applied to each node. To replicate the wave reflections seen experimentally, the phantom container was constrained in all directions. The mesh was primarily composed of structured hexahedron elements. Around the interfaces of the complex plaque geometry, unstructured tetrahedrons were used. The lumen was modelled using acoustic elements; all other components were modelled with hybrid elements. Through the stenosis, the element edge length was 0.5 mm, increasing to 1mm through the vessel wall and 2 mm through the tissue mimic. Data was extracted using a pixel size of 1.84 $mm^2$ by a slice thickness of 10 mm, mimicking the experimental resolution.

$$\sigma_{noise} = N\% \cdot \sigma_{signal} \quad (4)$$

Artificial noise $\sigma_{noise}$ was added at $N$=2% using Eq. 4, based on the standard deviation through the ROI $\sigma_{signal}$ with a Gaussian distribution and zero mean. The mean shear moduli were taken through the ROI and averaged over 20 noisy cycles.

## Inversion algorithm

The 2D Helmholtz equation describes harmonic wave propagation through an isotropic, homogeneous, incompressible, linear elastic medium in the absence of body forces [14]. This algorithm was used to invert the experimental and computational data sets (MATLAB R2011a, MathWorks, Natick, Massachusetts, USA). The algorithm, calculates the complex shear modulus $G(\omega)$, denoted in Eq. 1, from the Fourier transformed complex displacement $U$, the excitation frequency $\omega$, and the tissue density $\rho$.

$$G(\omega) = \frac{-\rho\omega^2 U}{\nabla^2 U} \quad (1)$$

$$G(\omega) = G'(\omega) + iG''(\omega) \quad (2)$$

$$G_{Voigt}(\omega) = \mu + i\omega\eta \quad (3)$$

The complex shear modulus is defined by Eq. 2. The shear modulus $\mu$, and shear viscosity $\eta$ are defined by the Voigt rheological model, Eq. 3. The application of this algorithm to atherosclerosis and the associated limitations are discussed in depth in Thomas-Seale et al. [24,39]. Noise and compression wave components were filtered using a 2D Butterworth filter [36,40]. Filter limits were explored by Thomas-Seale et al. [24]; it was concluded that over filtering of heterogeneous MRE data sets leads to a loss of the shear modulus contrast between compositions. Wide filter thresholds were set at 5 $m^{-1}$ and 1,000,000 $m^{-1}$.

# Results

## Arterial phantoms

Figure 3 captures the lumen in both the wave and elastogram images; however, the stenosis cannot be identified. Quantitative analysis of the shear moduli averaged through the phantom stenosis showed no differences between the stiffness of the plaques. The synthetic data in Figure 4 yields higher clarity images. The wave images show increased displacement through the plaque as the composition changes from fibrous to lipid.

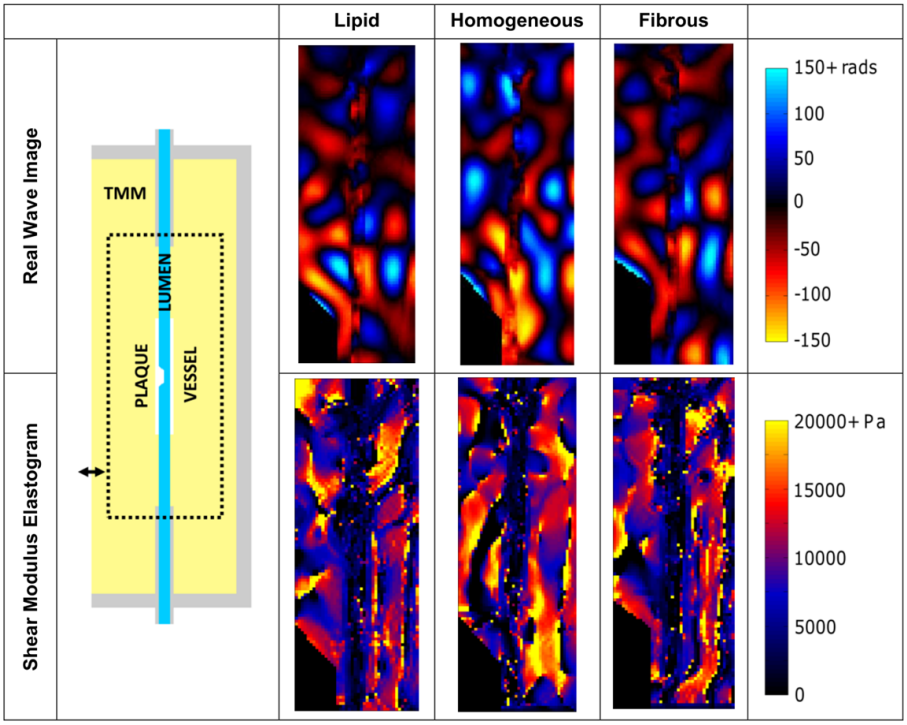


**Figure 3:** Waves images and elastograms through 70% stenosis arterial phantoms at each composition excited at 100 Hz and encoded through the read out motion (Y) direction.

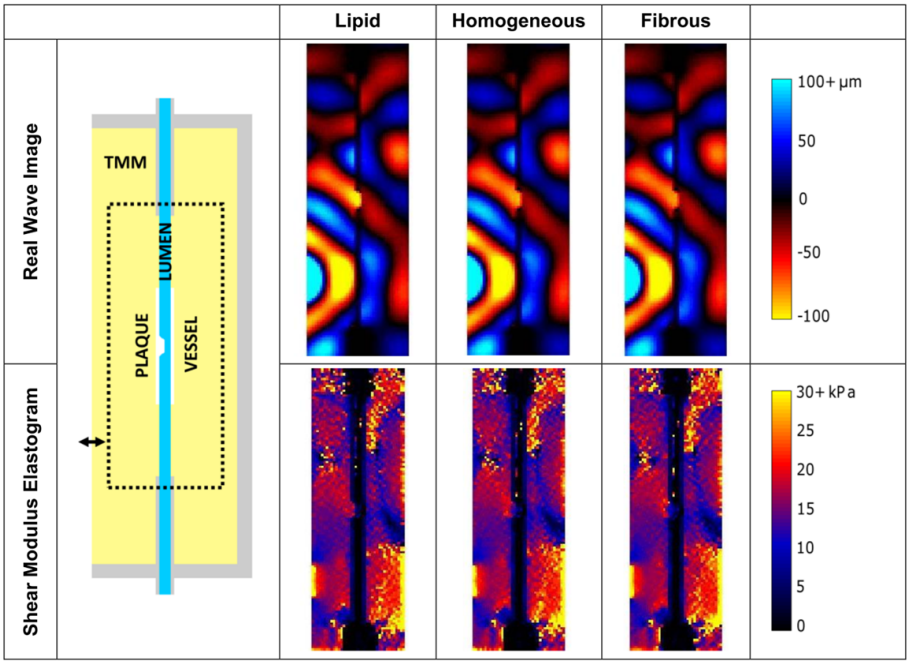


**Figure 4:** Waves images and elastograms through a synthetic 70% stenosis simulation at each composition excited at 100 Hz and encoded through the Y motion (RO) direction.

## Healthy volunteers and PAD patients

Figure 5 displays a selection of results from the healthy volunteers and patients. These images displayed the clearest propagation of waves through the ROI. The wave images and elastograms are accompanied by magnitude images which highlight the blood flow through the lumen. Overall the wave images and elastograms are poor quality, containing large amounts of noise. The lumen is visible in all the wave

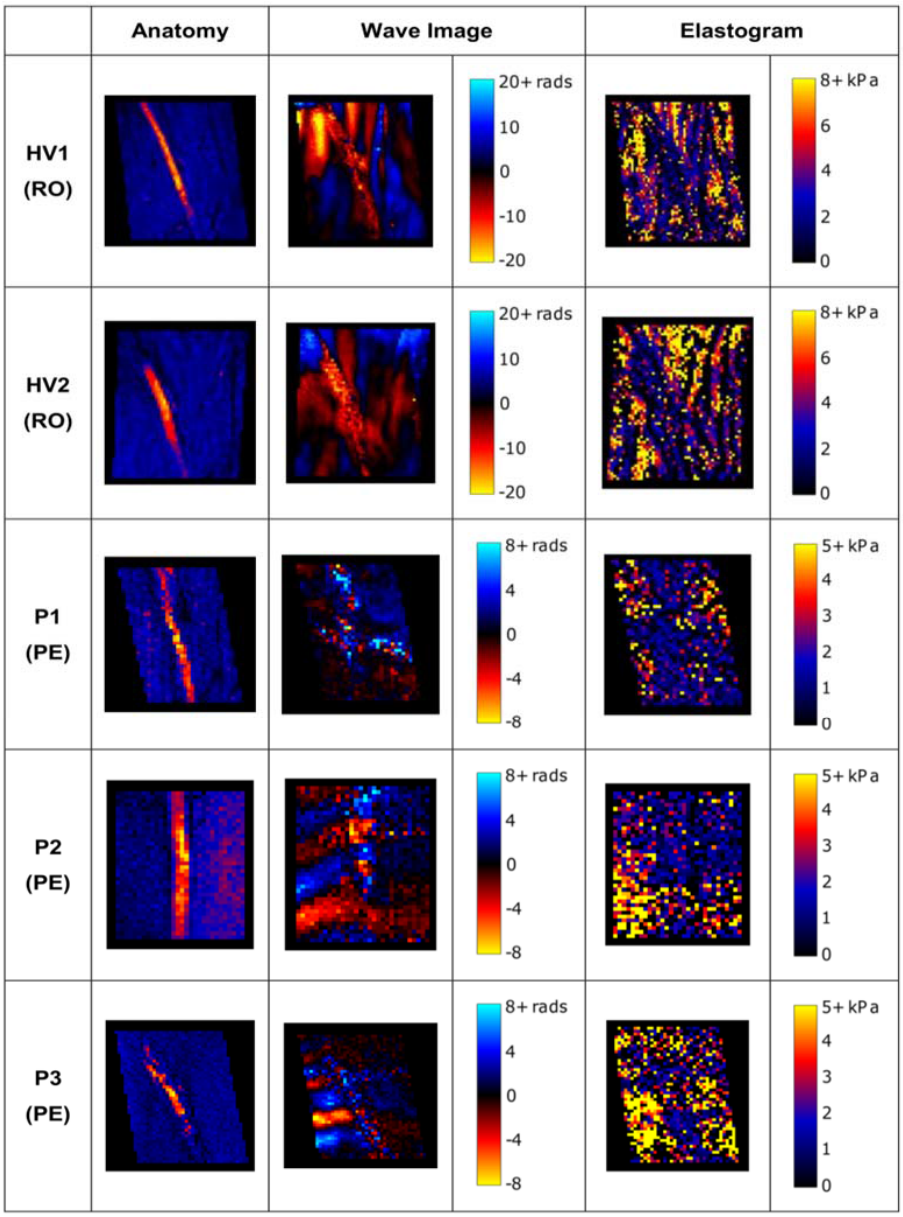


**Figure 5:** Wave images and elastograms for each subject through the specified motion encoding direction at 100Hz.

images; it can be identified in the healthy volunteer's elastograms but not the patient elastograms. The presence of disease cannot be detected in the patient wave images or elastogram images. However, there are identifiable differences between the healthy volunteer and patient wave images: the patient images are noisier, have lower amplitudes and the wave propagation is severely damped across the artery in comparison to the healthy volunteer images.

## Discussion

### Arterial phantoms

Although MRE was unable to identify the change in the mechanical properties of the plaque through the arterials phantoms, comparison of the experimental and computational methodology and results yields some interesting observations. The computational data sets contain more planar wave propagation and are not subject to imaging artefacts, particularly visible as ghosting artefacts in the background of the raw experimental images. This leads to clearer, more homogenous elastograms. Both heterogeneous systems were analyzed at the same resolution, contained multiple reflective boundaries, comparable noise levels and were excited using a compressional wave. The differences between the computational and experimental system is that the synthetic data does not contain imaging artefacts or wave disruptions from rigid body motion of the phantom or flow artefacts. This suggests that the experimental results could be improved through increased constraint of the phantom and the inclusion of a higher viscosity blood mimic.

### Healthy volunteers and PAD patients

From observation of quality of the elastograms generated by

the inversion of heterogeneous atherosclerotic experimental and computational [24] wave images, a subjective judgment was made as to the most promising data sets; ideal wave images will show good wave propagation through the ROI with a clear disruption along the lumen. In the case of Patient 2, MRE had to be conducted through a section of the vessel, slightly distal to the disease, due to the constraints of positioning the actuator.

To contextualize the results, similar to the arterial phantoms, differences would be expected between the patient and healthy volunteer data sets; areas of increased or decreased shear modulus along the wall of the vessel, would correlate with areas of either lipid or fibrous atherosclerotic disease. In this study, no quantitative differences can be seen between the healthy and diseased wave images and elastograms, however, some qualitative observations have been made.

Firstly, the patient images appear much noisier that the healthy volunteer images, they have lower wave amplitudes and were subject to some large motion artefacts, therefore the ROIs needed to be smaller. Overall the wave propagation through the healthy volunteers was clearer in the RO direction and for the patients in the PE direction. The image degradation could be due to increased physiological movement in the patients, compared to the more informed healthy volunteers. Some of the patient data sets were so corrupted by noise and imaging artefacts, that no wave propagation was visible. The study was not age matched. However, since PAD is more prevalent in the older population, there was a significant difference in the age range of the healthy volunteers and patients. Heterogeneity of the muscle stiffness has been shown to increase with age [41]. It is hypothesized that the increased age range of the patients led to more disputed wave interactions and artefacts generated by the inversion algorithm which is ill-suited to heterogeneous data sets [24].

In the majority of the healthy volunteer scans, the wave propagation on both sides of the vessel was equal. In the patient images, where there were identifiable waves, they are significantly clearer on the left hand side of the image. The wave images of the healthy volunteers and previous computational work [24] show minimal changes in wave amplitude across the lumen. Through this small sample size, this observation indicates that the presence of atherosclerosis and/or calcification, which can be severe in symptomatic PAD [42], may have damped the propagation of the waves through the artery. These conclusions require further investigation through a larger and repeated data set to be statistically significant.

This study was feasibility research, as such; the experimental data sets were not subject to any imaging parameter optimization or repetition. The presence of noise through MRE data disrupts the clarity of wave gradients and results in degradation in the accuracy of the technique [24]. Whilst use of the Butterworth filter through homogeneous images may be used to mitigate noise [36], Thomas-Seale et al. [24] noted that restrictive filter thresholds also smooth the essential contract through heterogeneous data sets. Therefore, the optimization of imaging parameters for optimum signal to noise ratio is of crucial importance. In addition, it can also be assumed that there were other sources of disruption to the images through artefacts created by physiological motion. The impact of this and/or the presence statistical outliers caused by artefacts cannot be identified due to the unrepeated nature of the study. The absence of repeated data also means that the findings in this study cannot be statistically quantified. The quality of the complex wave image depends on the temporal interaction of the excitation wave with the MRE imaging series. Any uncompensated motion in addition to the mechanical wave will interfere with its propagation. In this study the *in vivo* scans were not cardiac gated and hence the interaction of the wall motion and blood flow with the excitation wave and imaging sequence was not synchronized. Whilst statistically significant conclusions have been drawn utilizing imaging sequences without cardiac gating [19], the small, unrepeated sample size in this study makes it difficult to assess its impact and thus it is a limiting feature.

The inversion algorithm also imposed limitations on the study. These are discussed in detail by Thomas-Seale et al. [39,24]. In summary, the presence of boundaries, either naturally through a heterogeneous data set, an imaging boundary, or changes in the gradient of the data due to noise or artefacts, create step changes in the wave pattern which are magnified by the Laplacian opertator in the inversion algorithm. This leads to errors in the shear moduli resulting in pixelated and boundary artefacts through the data. This is an inherent limitation of the inversion algorithm and stems from it's application to a discrete, noisy and heterogeneous data set. The presence of additional artefacts created by physiological motion only serves to exasperate the issue. To progress this research beyond the preliminary data presented in this study, the acquisition parameters and inversion algorithm need to be optimized and adapted for cardiovascular applications, the data sets need to be both increased in size and studied over repeated acquisitions.

## Conclusions

The first application of MRE to atherosclerosis through arterial phantoms detected no differences with changing plaque composition in the wave images or elastograms, Synthetic modelling indicated that changes to the methodology of the technique could improve the results through the experimental arterial phantoms. Some qualitative differences were identified between the wave images of the healthy volunteers and patients. The most interesting result was the heavily damped wave propagation through the lumen of the PAD patient datasets, which may have been caused by the presence of atherosclerotic disease. The research requires further development to draw a firmer conclusion on the hypothesis; this includes an increased, repeatable data set and optimization of the imaging and inversion protocol.

## Compliance with Ethical Standards

All procedures performed in studies involving human participants were in accordance with the ethical standards of the institutional and/or national research committee and with the 1964 Helsinki declaration and its later amendments or comparable ethical standards. The study was conducted with the ethical approval of the South East Scotland Research Ethics Committee. Informed consent was obtained from all individual participants included in the study.

### Acknowledgements

This work was supported by the Engineering and Physical Sciences Research Council, The University of Edinburgh Innovation Initiative Grant and Chest Heart and Stroke Scotland Minor Research Award.

### Conflict of Interest

L. E. J. Thomas-Seale, P. Kennedy, L. Hollis, S. Hammer, T. Anderson, S. Mirsadraee, D. Klatt, I. Sack, P. Pankaj, N. Roberts and P. R. Hoskins declare that they have no conflict of interest.

### References

1. Go AS, Mozaffarian D, Roger VL, Benjamin EJ, Berry JD, et al. (2014) Heart disease and stroke statistics - 2014 update. A report from the American Heart Association. Circulation 129: E28-E292.

2. Vanepps JS, Vorp DA (2007) Mechano-pathobiology of atherogenesis: a review. J Surg Res 142: 202-217.

3. Libby P, Ridker PM, Maseri A (2002) Inflammation and atherosclerosis. Circulation 105: 1135-1143.

4. Stary HC, Chandler AB, Glagov S, Guyton JR, Insull W, et al. (1994) A definition of initial, fatty streak, and intermediate lesions of atherosclerosis - A report from the committee on vascular lesions of the council of arteriosclerosis, American Heart Association. Circulation 89: 2462-2478.

5. Stary HC, Chandler AB, Dinsmore RE, Fuster V, Glagov S, et al. (1995) A definition of advanced types of atherosclerotic lesions and a histological classification of atherosclerosis - A report from the committee on vascular lesions of the council on arteriosclerosis, American Heart Association. Circulation 92: 1355-1374.

6. Packard RR, Libby P (2008) Inflammation in atherosclerosis: from vascular biology to biomarker discovery and risk prediction. Clin Chem 54: 24-38.

7. Rothwell PM, Eliasziw M, Gutnikov SA, Fox AJ, Taylor DW, et al. (2003) Analysis of pooled data from the randomised controlled trials of endarterectomy for symptomatic carotid stenosis. Lancet 361: 107-116.

8. Falk E, Shah PK, Fuster V (1995) Coronary plaque disruption. Circulation 92: 657-671.

9. Bhatnagar P, Wickramasinghe K, Williams J, Rayner M, Townsend N (2015) The epidemiology of cardiovascular disease in the UK 2014. Heart 101: 1182-1189.

10. Corti R, Fuster V (2011) Imaging of atherosclerosis: magnetic resonance imaging. Eur Heart J 32: 1709-1719b.

11. de Korte CL, Hansen HH, van der Steen AF (2011) Vascular ultrasound for atherosclerosis imaging. Interface Focus 1: 565-575.

12. Mulder WJ, Jaffer FA, Fayad ZA, Nahrendorf M (2014) Imaging and nanomedicine in inflammatory atherosclerosis. Sci Transl Med 6: 239sr1.

13. Muthupillai R, Lomas DJ, Rossman PJ, Greenleaf JF, Manduca A, et al. (1995) Magnetic-resonance elastography by direct visualization of propagating acoustic strain waves. Science 269: 1854-1857.

14. Manduca A, Oliphant TE, Dresner MA, Mahowald JL, Kruse SA, et al. (2001) Magnetic resonance elastography: Non-invasive mapping of tissue elasticity. Medical Image Analysis 5: 237-254.

15. Woodrum DA, Romano AJ, Lerman A, Pandya UH, Brosh D, et al. (2006) Vascular wall elasticity measurement by magnetic resonance imaging. Magnetic Resonance in Medicine 56: 593-600.

16. Woodrum DA, Herrmann J, Lerman A, Romano AJ, Lerman LO, et al. (2009) Phase-contrast MRI-based elastography technique detects early hypertensive changes in ex vivo porcine aortic wall. J Magnetic Reson Imag 29: 583-587.

17. Xu L, Chen J, Yin M, Glaser KJ, Chen QS, et al. (2012) Assessment of stiffness changes in the ex vivo porcine aortic wall using magnetic resonance elastography. Magnetic Resonance Imaging 30: 122-127.

18. Xu L, Chen J, Glaser KJ, Yin M, Rossman PJ, et al. (2013) MR elastography of the human abdominal aorta: a preliminary study. J Magn Reson Imaging 38: 1549-1553.

19. Kolipaka A, Woodrum D, Araoz PA, Ehman RL (2012) MR elastography of the in vivo abdominal aorta: A feasibility study for comparing aortic stiffness between hypertensives and normotensives. J Magn Reson Imaging 35: 582-586.

20. Damughatla AR, Raterman B, Sharkey-Toppen T, Jin N, Simonetti OP, et al. (2015) Quantification of aortic stiffness using MR elastography and its comparison to MRI-based pulse wave velocity. J Magn Reson Imaging 41: 44-51.

21. Kenyhercz WE, Raterman B, Illapani VSP, Dowell J, Mo X, et al. (2016) Quantification of aortic stiffness using magnetic resonance elastography: measurement reproducibility, pulse wave velocity comparison, changes over cardiac cycle, and relationship with age. Magn Reson Med 75: 1920-1926.

22. Zhang N, Chen J, Yin M, Glaser KJ, Xu L, et al. (2016) Quantification of regional aortic stiffness using MR elastography: A phantom and ex-vivo porcine aorta study. Magn Reson Imaging 34: 91-96.

23. Thomas-Seale LEJ, Klatt D, Pankaj P, Roberts N, Sack I, et al. (2011) A simulation of the magnetic resonance elastography steady state wave response through idealised atherosclerotic plaques. IAENG Int J Comput Sci 38: 394-400.

24. Thomas-Seale LEJ, Hollis L, Klatt D, Sack I, Roberts N, et al. (2016) The simulation of magnetic resonance elastography through atherosclerosis. J Biomech 49: 1781-1788.

25. Dineley J, Meagher S, Poepping TL, McDicken WN, Hoskins PR (2006) Design and characterisation of a wall motion phantom. Ultrasound Med Biol 32: 1349-1357.

26. King DM, Moran CM, McNamara JD, Fagan AJ, Browne JE (2011) Development of a vessel-mimicking material for use in anatomically realistic doppler flow phantoms. Ultrasound Med Biol 37: 813-826.

27. Chu KC, Rutt BK (1997) Polyvinyl alcohol cryogel: An ideal phantom material for MR studies of arterial flow and elasticity. Magn Reson Med 37: 314-319.

28. Baldewsing RA, De Korte CL, Schaar JA, Mastik F, Van Der Steen AFW (2004) A finite element model for performing intravascular ultrasound elastography of human atherosclerotic coronary arteries. Ultrasound Med Biol 30: 803-813.

29. Pazos V, Mongrain R, Tardif JC (2010) Mechanical characterization of atherosclerotic arteries using finite-element modeling: Feasibility study on mock arteries. IEEE Trans Biomed Eng 57: 1520-1528.

30. Surry KJ, Austin HJ, Fenster A, Peters TM (2004) Poly(vinyl alcohol) cryogel phantoms for use in ultrasound and MR imaging. Phys Med Biol 49: 5529-5546.

31. Hamhaber U, Grieshaber FA, Nagel JH, Klose U (2003) Comparison of quantitative shear wave MR-elastography with mechanical compression tests. Magn Reson Med 49: 71-77.

32. Carstensen EL, Parker KJ, Lerner RM (2008) Elastography in the management of liver disease. Ultrasound Med Biol 34: 1535-1546.

33. Sinkus R, Lorenzen J, Schrader D, Lorenzen M, Dargatz M, et al. (2000) High-resolution tensor MR elastography for breast tumour detection. Phys Med Biol 45: 1649-1664.

34. Wang H, Weaver JB, Perreard II, Doyley MM, Paulsen KD (2011) A three-dimensional quality-guided phase unwrapping method for MR elastography. Phys Med Biol 56: 3935-3952.

35. Hamhaber U, Sack I, Papazoglou S, Rump J, Klatt D, et al. (2007) Three-dimensional analysis of shear wave propagation observed by in vivo magnetic resonance elastography of the brain. Acta Biomaterialia 3: 127-137.

36. Klatt D, Hamhaber U, Asbach P, Braun J, Sack I (2007) Noninvasive assessment of the rheological behavior of human organs using multifrequency MR elastography: a study of brain and liver viscoelasticity. Phy Med Biol 52: 7281-7294.

37. Hoskins PR (2010) Elastography, in Diagnostic Ultrasound: Physics and Equipment. P. R. Hoskins, K. Martin, and A. Thrush, (2nd edn), Cambridge University Press, Cambridge, UK.

38. Hoskins PR (2008) Simulation and validation of arterial ultrasound imaging and blood flow. Ultrasound Med Biol 34: 693-717.

39. Thomas-Seale LEJ (2015) The Application of Magnetic Resonance Elastography to Atherosclerosis,Thesis: Doctor of Philosophy, The University of Edinburgh, Edinburgh.

40. Clayton EH, Garbow JR, Bayly PV (2011) Frequency-dependent viscoelastic parameters of mouse brain tissue estimated by MR elastography. Phy Med Biol 56: 2391-2406.

41. Domire ZJ, McCullough MB, Chen QS, An KN (2009) Feasibility of using magnetic resonance elastography to study the effect of aging on shear modulus of skeletal muscle. J Appl Biomech 25: 93-97.

42. Hirsch AT, Haskal ZJ, Hertzer NR, Bakal CW, Creager MA, et al. (2006) ACC/AHA 2005 practice guidelines for the management of patients with peripheral arterial disease (lower extremity, renal, mesenteric, and abdominal aortic). Circulation 113: 463-654.